Self-Replicating Twins in Nanowires

Zaoshi Yuan[†,‡] and Aiichiro Nakano*[,†]

[†]Collaboratory for Advanced Computing and Simulations, Department of Physics and Astronomy, Department of Chemical Engineering and Materials Science, and Department of Computer Science, University of Southern California, Los Angeles, California 90089-0242, United States

[‡]Department of Chemical Engineering, Stanford University, Stanford, California 94305-5025, United States

S *Supporting Information*

ABSTRACT: Based on molecular-dynamics simulations validated with quantum-mechanical calculations, we predict that (111) twin planes in a [111]-oriented GaAs nanowire attain attractive interactions mediated by surface strain. This gives rise to a self-replication mechanism that continuously generates a twin superlattice in a nanowire during growth. We demonstrate significant implications of the twin−twin interaction for the electronic, mechanical, and chemical properties of nanowires. These unique properties suggest potential applications such as catalysts for solar fuel production and nanoscale mechanical dampers.

KEYWORDS: *Nanowire, twin−twin interaction, surface strain, GaAs, molecular dynamics*
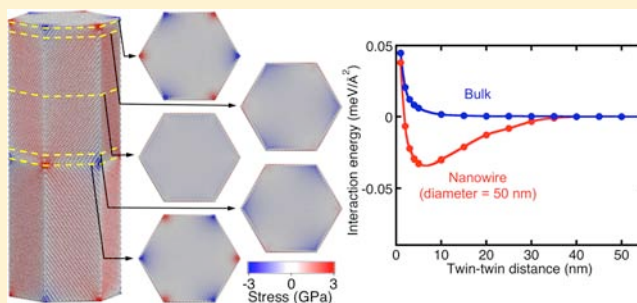
Due to their unique physical properties, nanowires (NWs) have broad applications such as sensors,[1] solar cells,[2] and high-strength/high-ductility material components.[3] A major issue in the application of semiconductor NWs is the high density of twin defects that are commonly observed.[4] Twins can be generated during growth (in the case of III−V semiconductor NWs[4−7]) or by deformation under shear (in the case of metals[8−10]). For III−V NWs, previous theoretical studies have identified corners on a NW top surface as preferred nucleation sites of stacking defects such as twins.[11,12] Since these corners are inevitable features of the NW geometry, stacking defects are inherent in NWs under most growth conditions.[12,13] Among various possible stacking defects (e.g., intrinsic and extrinsic stacking faults), twins are dominant in III−V NWs due to their small formation energy.[14] Not only do these twins essentially affect the electronic[15] and mechanical[16] properties of NWs, but they also provide an ideal tool to probe fundamental material processes at the nanometer scale. In particular, researchers studying NWs are uniquely positioned to address a fundamental scientific question: How twin defects interact with surfaces and other twins at the nanoscale?

Such twin−surface and twin−twin interactions are expected to play an essential role for determining material properties in NWs due to their high surface/volume ratios and short twin−twin distances (approximately a few nanometers).[4] Surface relaxation inherent in NWs gives rise to novel physical phenomena such as size-induced brittle-to-ductile transition in semiconductors[17] and metallic glasses.[18] Furthermore, sidewall-surface relaxation in ZnO NWs leads to an intrinsic core/shell structural transformation, that is, spontaneous formation of a radial heterostructure consisting of a hexagonal core and a body-centered tetragonal shell under tension.[19]

Cross-sectional scanning tunneling microscopy (XSTM) revealed atomic-scale relaxation of surfaces near twin planes in GaAs.[20] Such twin-induced surface relaxation likely interferes with the inherent surface relaxation in NWs mentioned above. This twin−surface interaction could in turn mediate interaction between twins, but such a possibility has not been examined to date either experimentally or theoretically.

Here, molecular-dynamics (MD) simulations validated with quantum-mechanical (QM) calculations reveal the existence of novel surface-mediated twin−twin attraction in NWs, which is nonexistent in bulk material (MD and QM methods are described in the Supporting Information). We will show that structural relaxation of the sidewall surfaces of a NW leads to spontaneous formation of an intrinsic core/shell structure. The associated inherent strain in the shell is relieved by the introduction of twin-boundary planes. The resulting surface stress-mediated interaction between twin planes exhibits attraction for a range of the NW diameter and twin−twin distance. The twin−twin interaction gives rise to a self-replication mechanism that continuously generates a twin superlattice in a NW during growth. This physical mechanism provides an alternative synthetic route for twin superlattices in NWs, in addition to geometrical routes proposed for some of the experimentally observed twin superlattices.[5−7] We will demonstrate significant implications of the twin−twin inter-action for the electronic, mechanical, and chemical properties of NWs, in conformity with a number of recent experimental

observations. These unique properties suggest potential applications such as catalysts for solar fuel production[21] and nanoscale mechanical dampers.[16]

We performed MD simulations of a GaAs NW, where the NW axis is the [111] orientation of zinc-blende (ZB) crystal. The energetics of twins in a NW is determined by a subtle balance between the bulk, surface, and other geometric terms such as surface kinks. To simplify the geometry such that twin–surface and twin–twin interactions can be unambiguously delineated, we considered a hexagonal NW with six $\{1\bar{1}0\}$ sidewalls. Two sets of systems were simulated: without (Figure 1a and b) and with (Figure 1c and d) twin. There are two types
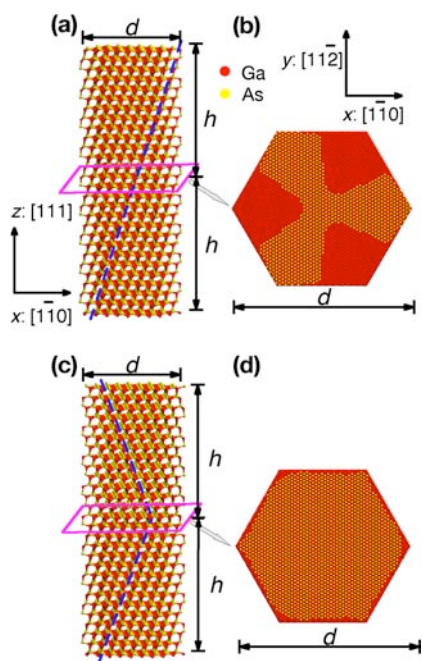

Figure 1. Simulated GaAs NWs. Red and yellow spheres represent Ga and As atoms, respectively, for NWs without (a and b) and with (c and d) twin. Parts a and c show side views, while b and d show top views of the atoms on the mid cross section (i.e., $z = h$ marked by magenta lines) of the NW. Dashed blue lines are added to show crystallographic orientations and their change at the twin boundary. In the top views in b and d, the topmost atoms (either Ga colored in red or As in yellow) below the $z = h$ plane are predominantly visible.

of twins: rotational (or ortho) and reflective (or para) twins. Rotational twins are dominant in ZB NWs. We thus introduced twin defects by rotating the upper half of the NW by 60°. Here, each rotational plane lies in the middle of a Ga monolayer below and an As monolayer above, which are narrowly separated and together form a GaAs bilayer (i.e., the rotational plane is a glide plane). This rotation reflects the stacking sequence of (111) crystalline planes at the twin-boundary plane, which is one-monolayer below the rotational plane and is located in the middle of two consecutive GaAs bilayers (i.e., the twin-boundary plane is a shuffle plane). With periodic boundary conditions (PBC) in the z (or [111]) direction, this procedure creates two (111) twin-boundary planes. For a NW of height $2h$, one twin plane is located at $z = h$ and the other at $z = 2h$ (or equivalently $z = 0$ due to PBC), with the twin-plane distance of h. By systematically changing the NW diameter d and twin–twin distance h, we were able to

investigate the effect of NW surfaces and the range of twin–twin interactions.

To study structural properties of twin boundaries, we first examined atomic displacements on the twin plane. Figure 1b and d are top views of atoms on the mid (i.e., $z = h$) cross section of the NW of diameter $d = 10$ nm without and with twin, respectively. The NW without twin in Figure 1b exhibits 3-fold symmetry, reflecting the 3-fold symmetry of ZB crystal around the [111] axis. Namely, Ga atoms (colored red) near three corners of the NW shift downward from above to below the mid shuffle plane to become visible in the top view of the $z = h$ cross section. On the other hand, atoms in the center do not shift, and those near the other three corners shift upward, which keeps As atoms (colored yellow) on the top. Such inhomogeneous displacements should not exist in bulk crystal, and therefore it is a consequence of the structural relaxation of the NW surface. Our previous MD study showed that such relaxation of NW sidewalls leads to the formation of an intrinsic core/shell structure; that is, a shell of 6–8 monolayers near NW sidewalls forms a distinct lattice structure from that in the inner core.[12,19] Such distinct phases at surfaces are akin to those well-established at interfaces. For example, grain-boundary interphases[22,23] known as complexions[24] essentially control material properties. Here, a thin layer of a metastable phase (which is not stable in bulk) becomes thermodynamically favorable, if the volumetric free energy to form the metastable phase is overcompensated by the reduction in the interfacial energy.[25] In contrast to the atomic displacements with 3-fold symmetry without twin (Figure 1b), those in the NW with twin (Figure 1d) are more symmetric and exhibit 6-fold symmetry on the twin plane. Twin thus modifies the inherent surface relaxation in a substantial way.

Because of the essential role played by the structural relaxation of the sidewall surfaces in subsequent discussions, we validated the MD result against QM calculation based on density functional theory (DFT). We computed the bond length as a function of the depth from the $(1\bar{1}0)$ surface in terms of the number of atomic layers using both MD and QM methods. While the bonds in the outermost two layers contract, the bonds in the third layer are elongated at a reduced magnitude. In both MD and QM calculations, the bond length converges to the bulk value at the seventh layer within 0.5%. In addition, the calculated MD results agree well with QM results for the lattice constants and cohesive energies of various crystalline phases, elastic constants, surface energies, vibrational density of states, thermal expansion coefficient, specific heat, and melting temperature.[26] These validations indicate the robustness of the simulation results presented in this paper.

To quantify the twin-plane structures, Figure 2 shows the displacement vector field on the mid cross section of the same NWs as shown in Figure 1. Each vector quantifies the displacement of an atom relative to their neighbors in the reference system (i.e., the system without relaxation). Top views of the NWs without (Figure 2a) and with (Figure 2c) twin show a core/shell structure similar to those previously observed.[12,19] Here, the outer shell exhibits larger displacements (colored red) compared to the inner core (colored blue). The corresponding side view in Figure 2b without twin shows alternating upward and downward shifts of the six NW corners, exhibiting the same 3-fold symmetry as in Figure 1b. Consequently, each (111) crystalline layer in the NW deforms into a buckled hexagon of a chairlike conformation shown in Figure 2b. Introduction of twin relieves these axial displace-
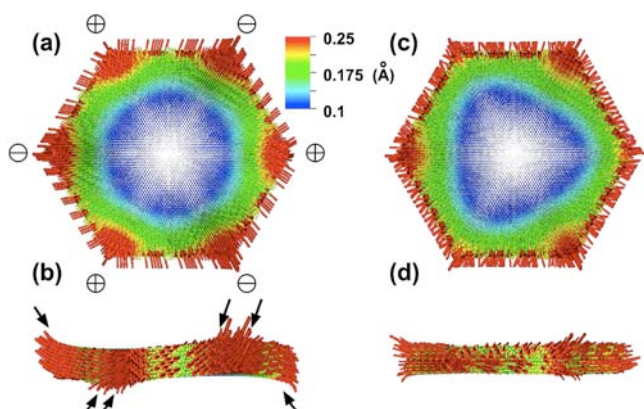
Figure 2. Effects of twin on atomic displacements in NWs. Parts a and b show top and side views of the displacement vector field on the mid plane (i.e., $z = h$) for NW without twin; c and d show the same information with twin. Each vector is represented with an arrow that points to an atomic position after relaxation, and its magnitude is color-coded. In a, the circles with plus and minus symbols represent upward and downward displacements of the six corners, respectively. In b, a black arrow represents the typical vector direction near each corner of the hexagon.

Figure 3. Twin-induced stress distribution in a NW. (a) Stress distribution with twin for $d = 20$ nm and $h = 25$ nm, where the hydrostatic stress is color-coded. (b and c) Cross-sectional views of stress sextupoles on the twin planes indicated by arrows. (d) Schematic of stress-mediated twin–twin interactions (double-headed arrows).

ments, and consequently the twin plane becomes a more planar hexagon shown in Figure 2d. Thus, structural relaxation of NWs is strongly modulated by the edges of the NW sidewall facets as well as their interaction with twin boundaries. This interaction between twins and surfaces is unique to NWs. Unlike their bulk counterparts, twins in NWs start and end at surfaces and interfere with the inherent structural relaxation of the NW surface. Similar atomic-scale surface relaxation associated with ortho twins has been observed by XSTM of a GaAs (110) surface.[20] The twin-induced change of symmetry from 3-fold to 6-fold explained above is concerned with the atomic displacements within the shell of the intrinsic core/shell structure. This is accompanied by an opposing change of symmetry in the core region. Namely, the small-deformation area represented by blue color is nearly circular without twin (Figure 2a), which becomes 3-fold symmetric with twin (Figure 2c).

The cooperative effects of twins and surfaces on the NW structure shown above are associated with strains and stresses. Figure 3a shows stress distribution in the NW with twin for $d = 20$ nm and $h = 25$ nm. We observe stress concentration at the corners of each hexagonal twin-boundary plane. The six corners exhibit alternating compressive and tensile stresses to form a stress sextupole (as seen in the cross-sectional views in Figure 3b and c. The twin boundary at the mid plane rotates the 3-fold symmetric atomic displacement (as shown in Figure 2b) by 60° between the upper and lower halves of the NW. At three of the six corners of the hexagonal twin plane, consequently, upward atomic displacements in the bottom twin segment and downward displacements in the top twin segment together create compressive stress (shown red in Figure 3c). At the other three corners, on the other hand, downward and upward displacements, respectively, in the bottom and top twin segments result in tensile stress (shown blue in Figure 3c). The stress sextupole on each twin plane is expected to bring in stress-mediated interaction between two twin planes as illustrated by arrows in Figure 3d. Not only do the corners of different twin planes interact, but also those within each twin plane have interaction. Due to the 60° rotation at each twin
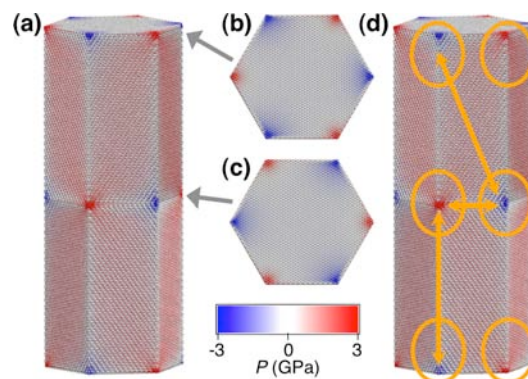
plane, in particular, consecutive twin planes have stress sextupoles of opposite signs. This may lead to attractive interaction between consecutive twin planes.

The stress-mediated twin–twin interaction mentioned above should be manifested in the dependence of the NW energy on the twin–plane distance h and diameter d. To investigate this, we performed MD simulations of various NWs by systematically changing h from 1 to 55 nm and d from 2 to 50 nm. In addition, we simulated the bulk limit (i.e., $d \to \infty$) by applying PBCs to all Cartesian directions with a lateral size of 2.77 nm × 3.20 nm in the x and y directions. For each combination of d and h, we performed MD simulations with and without twin. We then computed the energy difference ΔE by subtracting the NW energy without twin from that with twin. Figure 4a shows $\Delta E(d, h)$ as a function of h for the bulk limit, $d \to \infty$. We see that ΔE rapidly (within $h = 5$ nm) decreases and converges to the asymptotic limit at $h \sim 10$ nm. Here, the h dependence of ΔE reflects the bulk twin–twin interaction that has a short-range of ~ 5 nm, whereas the asymptotic ΔE value is twice the energy of a single twin boundary (since there are two twin boundaries in the NW). Glas used a simple heuristic to estimate the bulk twin energy for GaAs. Our MD result, $\Delta E(d \to \infty, h \to \infty) = 2.94$ meV/Å^2, compares reasonably with his semiempirical result, 2.1 meV/Å^2.[14]

To study the diameter dependence of the twin energy, Figure 4b plots $\Delta E(d, h \to \infty)$ (which is evaluated at $h = 55$ nm). With decreasing diameter, the twin energy decreases away from the bulk value (pointed by the arrow). Below a critical diameter of $d_c \sim 5.3$ nm, the twin energy becomes negative, making twin insertion an exothermic process. This is likely due to the strain relief by twin at the NW shell as shown in Figure 2. Below d_c, the resulting stress-release energy overcompensates the positive stacking-defect energy at the twin boundary to make twin insertion energetically favorable. A similar surface-induced mechanism was proposed for a structural transition from ZB to wurtzite (WZ) phase in GaAs NWs below a critical diameter.[27]

We define the twin–twin interaction energy by subtracting the isolated twin energies from ΔE: $E_{int}(d, h) = \Delta E(d, h) - \Delta E(d, \infty)$. Figure 4c and d shows E_{int} as a function of h for various d including the bulk limit ($d \to \infty$). In the bulk, the twin–twin interaction is purely repulsive as shown in Figure 4c. Below $d = 50$ nm, however, the interaction starts to have a
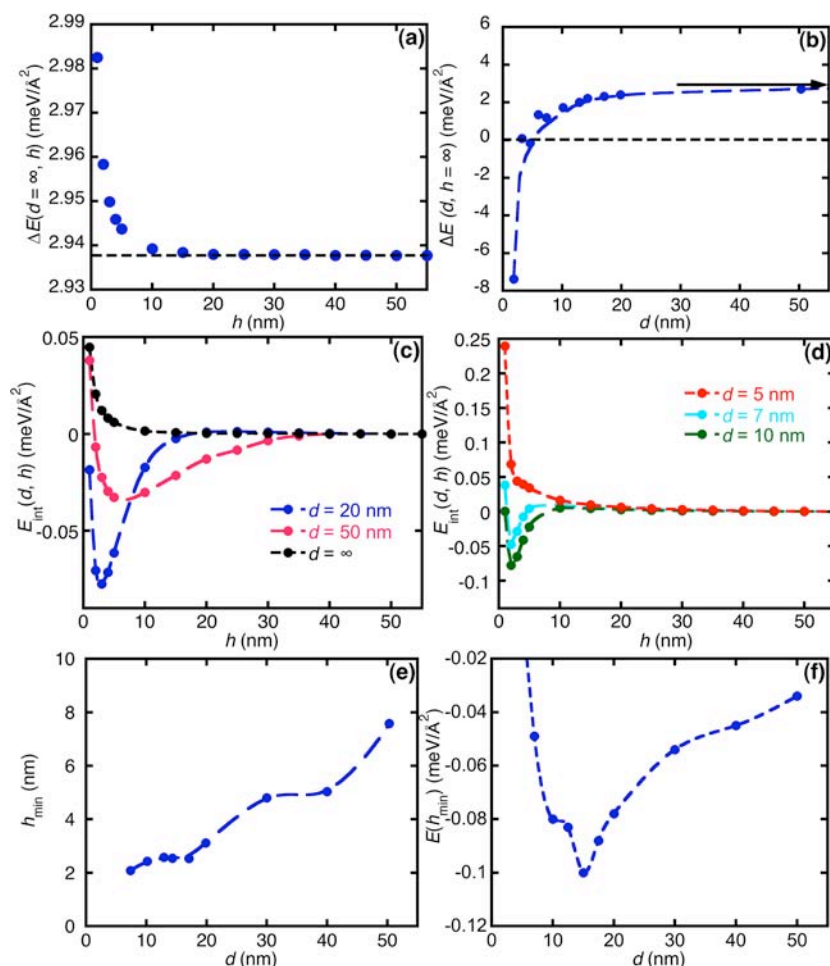
Figure 4. Energetics of twins in NWs. (a) The energy difference ΔE between NWs with and without twin as a function of the twin−twin distance h for the bulk limit, $d \rightarrow \infty$. The dashed line indicates the asymptotic value ($h \rightarrow \infty$). (b) The asymptotic ΔE for $h \rightarrow \infty$ as a function of the NW diameter d, where the arrow indicates the bulk value ($d \rightarrow \infty$). (c and d) Twin−twin interaction energy E_{int} as a function of h for $d = \infty$, 50, and 20 nm (c) and $d = 10$, 7, and 5 nm (d). (e) Minimum-energy twin−twin distance as a function of d. (f) Minimum twin−twin interaction energy as a function of d.

minimum and becomes attractive at distances larger than the minimum-energy distance h_{min}; see the curve for $d = 50$ nm in Figure 4c. The minimum interaction energy $E_{int}(h_{min})$ becomes more negative, and accordingly the twin−twin attraction becomes stronger for smaller diameters; see the curve for $d = 20$ nm in Figure 4c. Also, h_{min} becomes shorter for smaller diameters. This twin−twin attraction likely originates from the interaction between the stress sextupoles of opposite signs between consecutive twin planes as shown in Figure 3b and c. This in turn is a consequence of the interaction between twins and surfaces as explained before.

Figure 4d shows the twin−twin interaction energy for even smaller diameters. Below $d = 10$ nm, the minimum interaction energy turns back the trend and begins to be less negative. Finally, below $d = 5$ nm, the twin−twin interaction becomes purely repulsive again. As shown in Figure 4a, the twin−twin interaction in bulk is purely repulsive with a short-range of 5 nm. It is likely that the twin−twin interaction energy within 5 nm is dominated by the energy difference between different stacking sequences.[14] For extremely thin NWs, it is also conceivable that strain relief is insufficient to cause the stress-mediated twin−twin attraction. In short, twin−twin interaction undergoes a transition from purely repulsive to attractive below a critical NW diameter of $d_{c1} \sim 50$ nm; further reduction of the

diameter causes a reentrant transition to purely repulsive interaction at a second critical diameter of $d_{c2} \sim 5$ nm.

Mutually repulsive twins thus attain attractive interaction in NWs, which is akin to the theory of superconductivity,[28] where mutually repulsive electrons acquire attraction through distortion of the crystalline lattice. Since the twin interaction here originates from the relaxation of the crystalline lattice near NW sidewall surfaces, it is probably sensitive to the way the surface is terminated or coated. While the surface relaxation-induced twin−twin interaction is a generic phenomenon, how it is manifested in the energetics should depend on the surface geometry as well. For example, twins in NWs with {111} sidewalls introduce additional geometric features such as kinks, which affect the energetics significantly. In addition, these geometrically necessary twins are associated with polar sidewall surfaces, and thus its energetics involves a nontrivial electrostatic contribution and depends on Ga and As chemical potentials.[29] As mentioned before, we considered a NW with nonpolar cleavage {1$\bar{1}$0} sidewalls, which are free from such geometric and other energetic complications, and consequently twin−surface and twin−twin interactions can unambiguously be delineated and studied systematically.

The twin−twin attraction shown in Figure 4c and d has significant implications for a number of properties of NWs.

First, it affects the growth kinetics of NWs considerably. Kinetic models for defect formation in NWs are usually based on the change of Gibbs free energy for the nucleation of a defected island on a NW top surface.[11,12] Though these models consider the trade-off between the bulk and surface energies, defect–defect interaction has not been taken into account. To quantify this effect, let us consider the nucleation of a twinned hexagonal island on the (111)B top surface of a hexagonal GaAs NW.[12] At a typical growth temperature and vapor pressures for Ga and As, the critical diameter (above which the island grows indefinitely) for a defected island was estimated to be 5–20 nm.[12] The twin–twin interaction energy $E_{int}(h_{min})$ for $d = 20$ nm in Figure 4c is -0.0774 meV/Å^2. This lowers the Gibbs free energy of the critical twinned nucleus by 0.335 eV, with the corresponding increase of the probability for twin formation by a factor of 50 at a growth temperature of 1000 K. While the growth kinetics of twins in NWs is thus governed by the nucleation of a critical defect island (which in turn depends on the adatom energetics), twin formation under mechanical loading is instead dictated by the energy barrier for stacking-fault generation. To confirm that our MD model also describes the latter process correctly, we have calculated the unstable stacking fault energy (i.e., the energy barrier to slide a (111) glide plane). The MD result, 2.37 J/m^2, is in reasonable agreement with the QM result based on DFT, 2.71 J/m^2 (see Table S1 in the Supporting Information).

The twin–twin attraction thus suggests a self-replication mechanism for twin generation. Namely, once the first twin plane is introduced during the growth of a NW, a subsequent generation of twin planes becomes exothermic and self-sustained. The twin–twin attraction also has a measurable consequence on the twin-plane distance statistics; that is, the twin-distance distribution $p(h)$ is expected to have a peak at h_{min} because of the correlated twin generation due to the twin–twin attraction. This is in contrast to the case where such correlation is absent; then $p(h)$ follows the monotonically decreasing Poisson distribution. Experimentally observed $p(h)$ in similar materials, GaP and InP, indeed shows a peak, supporting correlated twin generation.[5,6] Figure 4e shows that h_{min} is an increasing function of d. The same trend was observed for the peak position of $p(h)$ in InP.[6] In particular, the experimentally measured average twin distance is ~2 nm for a NW diameter of ~10 nm,[6] which is consistent with our simulation result in Figure 4e (e.g., $h_{min} = 2.4$ nm for $d = 10$ nm). Figure 4f shows the minimum energy as a function of d. The magnitude of the minimum energy peaks at $d = 15$ nm, indicating that the twin–twin interaction in NWs has the strongest effect around this diameter. This physical mechanism for self-replicating twins is complementary to the generation of geometrically necessary twins during growth using the selective-area metal–organic vapor-phase epitaxy[4] or the vapor–liquid–solid method.[5–7] As such, it provides an alternative synthetic route for twin superlattices in NWs.[5–7] Such a controlled crystal structure and stacking-defect distribution in NWs provide a capability to tune their electronic, optical, and mechanical properties, thereby add a rich design space for NW-based devices.

Twin superlattices also affect the electronic properties of NWs. Our QM calculation based on DFT revealed a surprising effect of a twin superlattice; that is, it increases the radiative decay time of a bound exciton in a [111] oriented GaAs NW.[30] Here, the dipole oscillator strengths were computed between the wave functions at the conduction- and valence-band edges.

The oscillator strengths were then used to estimate the radiative decay time. For a twin-boundary distance of $h = 4$ nm, the lifetime increases by 6%. The enhanced charge-recombination lifetime is likely due to the spatial separation of electron and hole wave functions because of the twin-boundary potential. A similar electron–hole separation was predicted theoretically for tapered silicon NWs.[31] Experimentally, the reduction of the oscillator strength was observed in GaN/Al_xGa_{1-x}N quantum wells, where the separation of electron and hole wave functions is caused by the piezoelectric field.[32]

We also studied the effect of twin superlattices on carrier mobility. We first estimated the electronic scattering potential by a twin boundary by subtracting the local Kohn–Sham potential in DFT without twin boundary from that with a twin boundary. We then computed the transmission coefficient for this scattering potential as a function of the electron momentum. The electron mean-free path and scattering time were then derived from the transmission coefficient.[33] For the twin distance of $h = 1$ nm, the calculated twin-scattering contribution to electron mobility is 1600 cm^2/(V·s) at a temperature of 300 K.[30] This is consistent with recent terahertz photoconductivity measurements by Parkinson et al.[15] By eliminating twin defects, they observed the enhancement of the intrinsic carrier mobility from 1200 to 2250 cm^2/(V·s) for GaAs NWs of diameter 40–60 nm.[15] This implies the twin scattering contribution on the order of $\sim 2 \times 10^3$ cm^2/(V·s). Room-temperature electron mobilities in high-quality GaAs samples are $\sim 10^4$ cm^2/(V·s) (with the corresponding mean free path of $\sim 10^2$ nm), for which the dominant contribution is the scattering by optical phonons.[34] The estimated twin-scattering contribution is more significant for $h < 5$ nm. In addition to acting as a carrier-scattering source, twins in NWs were found to modify the mobility by changing strain and thereby the effective mass.[30] Namely, a few percent of strain modification due to twins (which is associated with the surface deformation shown in Figure 2) results in up to 80% of the mobility change, thereby significantly modulating the carrier transport in NWs.[30]

In addition to the electronic properties, the stress associated with twins in NWs (see Figure 3) is expected to influence surface chemistry and mechanics as well. It has been well-recognized that surface features such as steps and kinks are essential for catalytic activities of surfaces.[35] In particular, twins terminating at a surface were shown to endow the surface with enhanced catalytic capabilities.[36,37] Twins are expected to enhance the reactivity of NW surfaces not only through these geometric effects but also due to the stress associated with them as shown in Figure 3. Such effects of stress on surface reactivity were in fact demonstrated in recent experiments by Herbert et al.[38] They observed a dramatic increase of the reactivity with oxygen due to the residual strain near a dislocation on a nickel (100) surface. Similar mechanochemical effects may also play a role in recently observed spontaneous alloy ordering at the six edges of hexagonal GaAs NWs coated with Al_xGa_{1-x}As shells.[39] Due to these enhanced chemical activities, twin supperlattices in NWs may find novel applications such as solar fuel production.[21] In addition, stacking faults such as twins cause unusual mechanical properties of NWs, a notable example being an anelasticity (i.e., delayed recovery of elastic strain after the removal of an applied stress) of GaAs NWs, with potential applications such as nanoscale damping systems.[16]

In summary, twins acquire attractive interaction in NWs through atomic distortion of NW sidewall surfaces. The transition from purely repulsive to attractive twin–twin

interaction for decreasing NW diameters is followed by a reentrant transition to purely repulsive interaction again for even thinner NWs. These fundamental twin−twin and twin−surface interactions provide powerful means for self-assembly of nanostructures. The proposed intrinsic core/shell structure and twin−twin interaction also provide a conceptual framework to address broad issues regarding NWs, ranging from their unique thermomechanical properties[19] to defect-generation control.[12] This work thus lays a foundation for future studies of fundamental defect−defect and defect−surface interactions in nanostructures.

■ ASSOCIATED CONTENT

Ⓢ Supporting Information

Technical details of the MD simulation and QM calculation methods. This material is available free of charge via the Internet at http://pubs.acs.org.

■ AUTHOR INFORMATION

Notes

The authors declare no competing financial interest.

■ ACKNOWLEDGMENTS

■ REFERENCES

(1) Cui, Y.; Wei, Q. Q.; Park, H. K.; Lieber, C. M. *Science* **2001**, *293*, 1289−1292.

(2) Wallentin, J.; Anttu, N.; Asoli, D.; Huffman, M.; Aberg, I.; Magnusson, M. H.; Siefer, G.; Fuss-Kailuweit, P.; Dimroth, F.; Witzigmann, B.; Xu, H. Q.; Samuelson, L.; Deppert, K.; Borgstrom, M. T. *Science* **2013**, *339*, 1057−1060.

(3) Jang, D. C.; Li, X. Y.; Gao, H. J.; Greer, J. R. *Nat. Nanotechnol.* **2012**, *7*, 594−601.

(4) Tomioka, K.; Yoshimura, M.; Fukui, T. *Nature* **2012**, *488*, 189−192.

(5) Xiong, Q. H.; Wang, J.; Eklund, P. C. *Nano Lett.* **2006**, *6*, 2736−2742.

(6) Algra, R. E.; Verheijen, M. A.; Borgstrom, M. T.; Feiner, L. F.; Immink, G.; van Enckevort, W. J. P.; Vlieg, E.; Bakkers, E. P. A. M. *Nature* **2008**, *456*, 369−372.

(7) Caroff, P.; Dick, K. A.; Johansson, J.; Messing, M. E.; Deppert, K.; Samuelson, L. *Nat. Nanotechnol.* **2009**, *4*, 50−55.

(8) Ogata, S.; Li, J.; Yip, S. *Science* **2002**, *298*, 807−811.

(9) Yu, Q.; Shan, Z. W.; Li, J.; Huang, X. X.; Xiao, L.; Sun, J.; Ma, E. *Nature* **2010**, *463*, 335−338.

(10) Chen, H.; Kalia, R. K.; Kaxiras, E.; Lu, G.; Nakano, A.; Nomura, K.; van Duin, A. C. T.; Vashishta, P.; Yuan, Z. *Phys. Rev. Lett.* **2010**, *104*, 155502.

(11) Glas, F.; Harmand, J. C.; Patriarche, G. *Phys. Rev. Lett.* **2007**, *99*, 146101.

(12) Yuan, Z.; Nomura, K.; Nakano, A. *Appl. Phys. Lett.* **2012**, *100*, 163103.

(13) Chi, C.-Y.; Chang, C.-C.; Hu, S.; Yeh, T.-W.; Cronin, S. B.; Dapkus, P. D. *Nano Lett.* **2013**, *13*, 2506−2515.

(14) Glas, F. *J. Appl. Phys.* **2008**, *104*, 093520.

(15) Parkinson, P.; Joyce, H. J.; Gao, Q.; Tan, H. H.; Zhang, X.; Zou, J.; Jagadish, C.; Herz, L. M.; Johnston, M. B. *Nano Lett.* **2009**, *9*, 3349−3353.

(16) Chen, B.; Gao, Q.; Wang, Y.; Liao, X.; Mai, Y.-W.; Tan, H. H.; Zou, J.; Ringer, S. P.; Jagadish, C. *Nano Lett.* **2013**, *13*, 3169−3172.

(17) Ostlund, F.; Rzepiejewska-Malyska, K.; Leifer, K.; Hale, L. M.; Tang, Y. Y.; Ballarini, R.; Gerberich, W. W.; Michler, J. *Adv. Funct. Mater.* **2009**, *19*, 2439−2444.

(18) Jang, D. C.; Greer, J. R. *Nat. Mater.* **2010**, *9*, 215−219.

(19) Yuan, Z.; Nomura, K.; Nakano, A. *Appl. Phys. Lett.* **2012**, *100*, 153116.

(20) Bolinsson, J.; Ouattara, L.; Hofer, W. A.; Skold, N.; Lundgren, E.; Gustafsson, A.; Mikkelsen, A. *J. Phys.: Condens. Matter* **2009**, *21*, 055404.

(21) Liu, C.; Tang, J.; Chen, H. M.; Liu, B.; Yang, P. *Nano Lett.* **2013**, *13*, 2989−2992.

(22) Szlufarska, I.; Nakano, A.; Vashishta, P. *Science* **2005**, *309*, 911−914.

(23) Shimamura, K.; Shimojo, F.; Kalia, R. K.; Nakano, A.; Vashishta, P. *Phys. Rev. Lett.* **2013**, *111*, 066103.

(24) Dillon, S. J.; Tang, M.; Carter, W. C.; Harmer, M. P. *Acta Mater.* **2007**, *55*, 6208−6218.

(25) Luo, J. *Crit. Rev. Solid State Mater. Sci.* **2007**, *32*, 67−109.

(26) Kodiyalam, S.; Kalia, R. K.; Nakano, A.; Vashishta, P. *Phys. Rev. Lett.* **2004**, *93*, 203401.

(27) Akiyama, T.; Sano, K.; Nakamura, K.; Ito, T. *Jpn. J. Appl. Phys. Pt 2* **2006**, *45*, L275−L278.

(28) Bardeen, J.; Cooper, L. N.; Schrieffer, J. R. *Phys. Rev.* **1957**, *108*, 1175−1204.

(29) Moll, N.; Kley, A.; Pehlke, E.; Scheffler, M. *Phys. Rev. B* **1996**, *54*, 8844−8855.

(30) Shimamura, K.; Yuan, Z.; Shimojo, F.; Nakano, A. *Appl. Phys. Lett.* **2013**, *103*, 022105.

(31) Wu, Z. G.; Neaton, J. B.; Grossman, J. C. *Phys. Rev. Lett.* **2008**, *100*, 246804.

(32) Im, J. S.; Kollmer, H.; Off, J.; Sohmer, A.; Scholz, F.; Hangleiter, A. *Phys. Rev. B* **1998**, *57*, R9435−R9438.

(33) Lee, H.; Choi, H. J. *Nano Lett.* **2010**, *10*, 2207−2210.

(34) Singh, J. *Electronic and Optoelectronic Properties of Semiconductor Structures*; Cambridge University Press: Cambridge, UK, 2007.

(35) Norskov, J. K.; Bligaard, T.; Rossmeisl, J.; Christensen, C. H. *Nat. Chem.* **2009**, *1*, 37−46.

(36) Behrens, M.; Studt, F.; Kasatkin, I.; Kuhl, S.; Havecker, M.; Abild-Pedersen, F.; Zander, S.; Girgsdies, F.; Kurr, P.; Kniep, B. L.; Tovar, M.; Fischer, R. W.; Norskov, J. K.; Schlogl, R. *Science* **2012**, *336*, 893−897.

(37) Liu, M.; Jing, D.; Zhou, Z.; Guo, L. *Nat. Commun.* **2013**, *4*, 2278.

(38) Herbert, F. W.; Van Vliet, K. J.; Yildiz, B. *MRS Commun.* **2011**, *2*, 23−27.

(39) Rudolph, D.; Funk, S.; Doblinger, M.; Morkotter, S.; Hertenberger, S.; Schweickert, L.; Becker, J.; Matich, S.; Bichler, M.; Spirkoska, D.; Zardo, I.; Finley, J. J.; Abstreiter, G.; Koblmuller, G. *Nano Lett.* **2013**, *13*, 1522−1527.